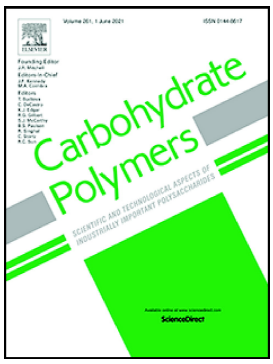

Starch hydrogels as targeted colonic drug delivery vehicles

Todor T. Koev, Hannah C. Harris, Sara Kiamehr, Yaroslav Z. Khimyak, Frederick J. Warren

PII: S0144-8617(22)00317-4

DOI: https://doi.org/10.1016/j.carbpol.2022.119413

Reference: CARP 119413

To appear in: *Carbohydrate Polymers*

Received date: 22 October 2021

Revised date: 22 March 2022

Accepted date: 23 March 2022

Please cite this article as: T.T. Koev, H.C. Harris, S. Kiamehr, et al., Starch hydrogels as targeted colonic drug delivery vehicles, *Carbohydrate Polymers* (2021), https://doi.org/10.1016/j.carbpol.2022.119413

Starch Hydrogels as Targeted Colonic Drug Delivery Vehicles

Todor T. Koev [1,2], Hannah C. Harris [2], Sara Kiamehr[1], Yaroslav Z. Khimyak [1], Frederick J. Warren[2]

1. School of Pharmacy, University of East Anglia, Norwich Research Park, NR4 7TJ (UK)

2. Food Innovation and Health, Quadram Institute Bioscience, Norwich Research Park, NR4 7UQ (UK)

Abstract

Targeted colonic drug delivery systems are needed for the treatment of endemic colorectal pathologies, such as Crohn's disease, ulcerative colitis, and colorectal cancer. These drug delivery vehicles are difficult to formulate, as they need to remain structurally intact whilst navigating a wide range of physiological conditions across the upper gastrointestinal tract. In this work we show how starch hydrogel bulk structural and molecular level parameters influence their properties as drug delivery platforms. The *in vitro* protocols mimic *in vivo* conditions, accounting for physiological concentrations of gastrointestinal hydrolytic enzymes and salts. The structural changes starch gels undergo along the entire length of the human gastrointestinal tract have been quantified, and related to the materials' drug release kinetics for three different drug molecules, and interactions with the large intestinal microbiota. It has been demonstrated how one can modify their choice of starch in order to fine tune its corresponding hydrogel's pharmacokinetic profile.

Key Words

Starch Hydrogels

Colorectal Drug Delivery

Gut Bacteria

NMR Spectroscopy

Short-chain Fatty Acids

Metabolomics

Abbreviations

NM – normal maize

H7 – Hylon VII® maize

VNL – Vanillin

5FU – 5-Fluorouracil

DOX – Doxorubicin

NMR – nuclear magnetic resonance

GIT – gastrointestinal tract

CP/MAS – cross polarisation magic angle spinning

CPSP/MAS – cross polarisation single-pulse magic angle spinning

HR-MAS – high resolution magic angle spinning

STD – saturation transfer difference

BP – British Pharmacopoeia

SCFAs – Short-chain fatty acids

1. Introduction

Orally administrable targeted colonic drug delivery systems have been of great scientific interest over the past decade (Amidon, Brown, & Dave, 2015; Bagliotti Meneguin, Stringhetti Ferreira Cury, & Evangelista, 2014), due to their potential to improve the administration of currently existing treatments for common colorectal pathologies (*e.g.*, ulcerative colitis, Crohn's disease, colorectal cancer). This is largely achieved by providing localised release and distribution of drug molecules at higher concentrations in the colon, whilst limiting upper gastrointestinal tract (GIT) drug release, systemic absorption, and metabolism. Drug carriers' structural integrity has a significant impact on their role as excipients, as well as on the pharmacokinetic profile of the loaded drug molecules. Depending on the primary mode of drug delivery – either drug diffusion dominated, or matrix disintegration-dominated, structural integrity and matrix organisation play a major role in achieving optimal release kinetics (Peppas, Bures, Leobandung, & Ichikawa, 2000).

At present, the most promising candidates for orally administrable targeted colonic pharmaceutical excipients are biocompatible natural polysaccharides such as starch, cellulose and pectins (Varum, Freire, Bravo, & Basit, 2020). Hydrothermally treated and subsequently retrograded starch forms hydrogel structures able to resist small intestinal digestion (resistant starch type III, RS III)(Edwards et al., 2015; Englyst, Kingman, & Cummings, 1992; Silvester, Englyst, & Cummings, 1995), and reach the colon structurally intact, where they are fermented by commensal bacteria (Raigond, Ezekiel, & Raigond, 2015; Topping & Clifton, 2001). There has been some research on the impact of starch on the gut microbiota (Le Leu et al., 2007; Topping & Clifton, 2001; Warren, Fukuma, Mikkelsen, Flanagan, & Williams, 2018), but not much is known about the structure-function relationships governing starch hydrogels' interaction and impact on the full extent of the GIT (Koev, Muñoz-García, Iuga, Khimyak, & Warren, 2020).

The human GIT (oral, small and large intestinal) microbiome has been shown to be populated by tens of trillions of microorganisms, providing its host with physiologically relevant enzymes, not natively secreted by the host (Cerf-Bensussan & Gaboriau-Routhiau, 2010; Cryan & O'Mahony, 2011; Kaoutari, Armougom, Gordon, Raoult, & Henrissat, 2013; Purchiaroni et al., 2013). Many gut bacteria have been shown to be capable of starch fermentation and/or degradation (Kaoutari et al., 2013). RS fermented in the large intestine has been shown to lead to the production of gases, short-chain fatty acids (SCFAs) and low levels of alcohols (Flint, Scott, Duncan, Louis, & Forano, 2012). Gut bacteria-mediated amylolysis is a result of the combined action of α-1,4- and α-1,6-specific enzymes (*i.e.*, type I pullulanases and amylopullulanases), originating from three major phyla – *Actinobacteria*, *Bacteroidetes* and *Firmicutes*, together accounting for 95% of the total mammalian gut microflora (Birt et al., 2013). Several important Gram-positive and negative microbial species, such as *Ruminococcus bromii*, *Bacteroides thetaiotaomicron and Bifidobacteria*, have been shown to be capable of both resistant starch degradation and of utilising partial products of starch digestion, such as di-, trisaccharides and maltodextrins (Reeves, D'Elia, Frias, & Salyers, 1996; Ze et al., 2015). Most British Pharmacopoeia (BP) utilised methods of simulating solid dosage forms' dissolution and disintegration under *in vitro* conditions focus primarily on the gastric or small intestinal environments (Bisharat, Barker, Narbad, & Craig, 2019). This approach fails to account for physiological concentrations of hydrolytic enzymes and salts across the human upper GIT, leading to an overestimation of the ability of pharmaceutical excipients to reach the large intestine structurally intact.

In our previous work, we showed how amylose content and preparation methods dictate starch hydrogels' bulk and molecular level properties. Low-amylose containing starches, such as normal maize (NM) produced structurally weaker gels, with higher degree of molecular mobility, compared to high-amylose starch hydrogels, such as Hylon VII® (H7) (Koev et al., 2020). In this study, we probe the viability of NM and H7 starch hydrogels as orally administrable colonic drug delivery vehicles, linking gel structure with its functional properties in the human GIT. We integrate two widely accepted models of *in vitro* digestion (Brodkorb et al., 2019; Minekus et al., 2014) and colonic fermentation (Williams, Bosch, Boer, Verstegen, & Tamminga, 2005; Williams et al., 2015), accounting for *in vivo* concentrations of hydrolytic enzymes. Both *in vitro* models have been developed based on available *in vivo* human physiological data (Brodkorb et al., 2019; Williams et al., 2005). These models have been extensively validated against *in vivo* data (Egger et al., 2016, 2017; Sanchón et al., 2018), and provide an accurate and representative model of the human GIT. We provide a complete representation of the *in vivo* behaviour of starch gels as pharmaceutical excipients, compared to other works (Ali & Alarifi, 2009; Bagliotti Meneguin et al., 2014; Namazi, Fathi, & Dadkhah, 2011). We demonstrate how to use this insight for the design of hydrogel pharmaceutical excipients from easily accessible and affordable materials, which resist upper GIT degradation, and achieve sustained drug release confined exclusively to the colon.

Furthermore, we show how structure governs interactions of starch gel systems with host's commensal bacteria, and their ability to utilise the hydrogel excipient as a substrate for the production of important physiologically relevant

microbial metabolites, such as SCFAs (Le Gall et al., 2011; Lockyer & Nugent, 2017). To the best of our knowledge, this is the first work to apply the INFOGEST protocol of *in vitro* digestion, the batch colon model, as well as high-resolution NMR spectroscopy to the context of targeted colonic pharmaceutical excipients. Our work provides insight for the development of superior orally administrable targeted drug delivery platforms with auxiliary physiologically relevant properties.

2. Materials and methods

2.1 Materials

NM was purchased from Merck (formerly Sigma Aldrich, Darmstadt, Germany). H7 was kindly provided as a gift by Ingredion Incorporated (Manchester, UK, Table 1). All other compounds and reagents were purchased from Merck.

Human salivary alpha-amylase (CAS: 9000-90-2, A1031: type XIII-A lyophilized powder, AA from human saliva, 1357 IU per mg protein, 81% protein), pepsin from porcine mucosa (CAS: 9001-75-6, P7012: pepsin from porcine gastric mucosa, 2074 IU per mg enzyme), porcine pancreatin (CAS: 8049-47-6, P7545: pancreatin from porcine pancreas, 2422 IU amylase activity per mg enzyme) and bovine bile (CAS: 8008-63-7) and all other reagents were purchased from Merck (Dorset, UK).

Table 1. Whole molecular structural parameters and source of normal maize (NM) and Hylon VII® (H7) starch.

Starch Type	$R_{hAMpeak}$ (nm)	$R_{hAPpeak}$ (nm)	Source
NM	20	200	Merck
H7	12	300	Ingredion

2.2 Hydrogel preparation

Starch hydrogels (10% w/v) were prepared as previously described (Koev et al., 2020). In brief, gelatinisation and subsequent storage of all starch samples was performed by preparing 10% (w/v) starch/deionised water suspensions in 25.0 mL Pyrex® screw top vials, vortex mixed and autoclaved (121 °C, 15 psig) for 20 min, followed by storage for 8 days at 4 °C, forming opaque white gels (Table 2). All hydrogels intended for simulated digestion, fermentation and rheological analyses were carefully excised using a 10 mm cork borer (Breckland Scientific Supplies Ltd., Stafford, UK) and cut into cylinders, 10 mm in height, using a surgical blade (Swann Morton Ltd., Sheffield, UK).

Drug-loaded starch hydrogels were prepared by incorporating vanillin (VNL), 5-fluorouracil (5FU) and doxorubicin (DOX) at 1% (w/v) prior to gelatinisation. NM and H7 starch hydrogels containing the small molecules are referred to as NM-VNL, NM-5FU and NM-DOX, H7-VNL, H7-5FU and H7-DOX respectively (Table 2).

Table 2. Starch hydrogel contents, concentrations, and designations used throughout this work.

Hydrogel Reference	Normal Maize (% w/v)	Hylon VII® (% w/v)	Vanillin (% w/v)	5-Fluorouracil (% w/v)	Doxorubicin (% w/v)
NM	10	0	0	0	0
H7	0	10	0	0	0
NM-VNL	10	0	1	0	0
H7-VNL	0	10	1	0	0
NM-5FU	10	0	0	1	0
H7-5FU	0	10	0	1	0
NM-DOX	10	0	0	0	1
H7-DOX	0	10	0	0	1

2.3 INFOGEST in vitro digestion

Digestion was carried out in triplicate using a standardised static simulated digestion model developed by Minekus *et al*., 2014, which consists of an oral phase, featuring salivary α-amylase as a hydrolytic enzyme, a gastric phase (pepsin), and a small intestinal phase (pancreatin, Supplementary data). The original protocol was modified to substitute $NaHCO_3$ and $[NH_4]HCO_3$ with bis-tris (Petropoulou et al., 2020), due to the latter's higher buffering capacity in the range of pH 6.0 – 7.2 (Supplementary data).

2.3.1 Halting digestion & sample collection

At the end of each simulated phase and at the mid-point of both the simulated gastric and small intestinal digestion steps (oral, O; gastric, G1 and G2; duodenal, D1 and D2), vessels were removed from the incubator, and the pH was raised to pH 9.0 (± 0.5) using $NaHCO_3$ (1.0 M) to halt enzymatic activity. The partially digested hydrogel substrates were removed from the digestion mixture and placed in phosphate buffered saline (PBS, 0.01 M) containing NaN_3 (0.02% w/v) and stored at 4 °C until further analysis. The digesta were stored at -20 °C for further analysis.

2.4 Quantification of digested starch hydrogel

The starch hydrogel digesta were thawed out, vortex mixed for 10 s and spun down (Eppendorf Centrifuge 5810R) at 13,000 x g for 5 min, and the supernatant removed to a clean tube for analysis. The concentration of reducing sugars in the supernatant was analysed using the *para*-hydroxybenzoic acid hydrazine (*p*AHBAH) method against maltose standards (Moretti & Thorson, 2008). The absorbance was measured using a UV-Vis spectrophotometer (Biochrom Libra S50 UV/Vis Spectrophotometer, λ_{max} = 405 nm).

2.5 Identification of oligosaccharides and reducing sugars in starch digesta

The supernatants collected after spinning down the starch digesta were analysed on a Bruker Avance I spectrometer, operating at ^{1}H and ^{13}C frequencies of 500 and 125.79 MHz, equipped with a 5 mm probe. Aliquots of 600 μL were loaded into NMR tubes (Norell Inc.®). Direct ^{13}C detection with ^{1}H decoupling experiments were acquired with a 10 μs ^{13}C $\pi/2$ pulse, 4.0 s relaxation delay, a minimum of 256 scans, and carried out at 25 °C.

2.6 Batch fermentation and vessel sampling

2.6.1 Faecal sample collection and preparation for inoculation

Faecal samples were obtained from 4 different subjects (see participant information and ethics below). Each volunteer was given a sample collection kit with instructions. The samples were produced inside sterilised plastic bags, sealed with a plastic clip, and placed in sealed plastic containers within 2 h of inoculation. The containers were transferred to a sterilised class II safety cabinet (Walker Ltd, UK). An average of 30.0 g of donor stool sample was homogenised with sterile PBS (0.01 M) reduced in an anaerobic chamber overnight, in a ratio of 1:10, in a strainer bag (BA6141/STR, Seward Limited, UK) using a Stomacher® 400 Circulator (Seward Limited, UK) set to 200 r.p.m. for a duration of 30 s, resulting in diluted faecal slurry intended for inoculation.

2.6.2 Vessel sampling

Simulated fermentation experiments were performed following the methodology of Williams *et al*. with some adaptations (Supplementary data) (Williams et al., 2005). In brief, 100-mL sterile, septa-sealed fermentation vessels (76.0 mL basal solution, 5.0 mL vitamin-phosphate/carbonate solution, 1.0 mL sulfide reducing solution) containing pre-digested (INFOGEST-treated) starch hydrogels were placed under CO_2 for 3 min each, and were left to equilibrate in an incubator at 37.0 °C the evening before inoculation. On the following day, inoculation was performed by injecting diluted faecal slurry (3.0 mL) directly through the septa of each fermentation bottle, using sterile 19G hypodermic needles and 10.0 mL syringes. Inoculation was carried out in a class II safety cabinet. All vessels were returned to the incubator immediately following inoculation.

2.6.3 Measurement of total gas produced during fermentation

At pre-determined time points (12, 24, 48 and 72 h after inoculation) bottles were taken out of the incubator and the gas produced was measured directly through the septa, using sterile 19G needles and 20 mL syringes, where the volume of gas measured at each time point was equal to the volume in the syringe (*i.e.*, distance of the plunger) being displaced.

2.6.4 Samples for bacterial metabolite analysis

At pre-determined time points (0, 6, 12, 24, 48 and 72 h after inoculation) bottles were taken out of the incubator and the fermentation media was sampled (2.0 mL) in triplicate through the septa, using sterile 23G needles and 5.0 mL

syringes. The samples were placed in 2.0-mL screw-cap centrifuge tubes, spun down at 3,000 x g for 5 min at 4 °C (Thermo Heraeus Fresco 17 centrifuge). The supernatant was collected without disturbing the pellet, where both were retained and stored at -20.0 °C for further analyses.

2.6.5 Samples for NMR structural analyses, FISH and LSCM

At pre-determined time points (12, 24, 48 and 72 h following inoculation), vessels were removed from the incubator and placed in an ice bath for 10 min. The starch hydrogels intended for NMR analyses were tipped out into 5.0 mL sterile vessels containing $NaHCO_3$ (1.0 M), swirled gently for 1.0 min and placed under PBS (0.01 M), containing NaN_3 (0.02% w/v); and the hydrogels intended for hybridisation and microscopy – in sterile vessels containing cold (4.0 °C) formaldehyde (4.0% in 0.01 M PBS) and left in the fixative at 4.0 °C overnight. Hydrogel sampling was performed in duplicate for each time point of the *in vitro* fermentation.

2.7 Fluorescence *in-situ* hybridisation (FISH)

The fixed hydrogel samples were removed from the formaldehyde solution, placed in 2.5 mL embedding plastic boats, and covered in mounting medium (PolyFreeze O.C.T. medium, Merck SHH0026). The embedding boats were gently placed in an EtOH/dry ice bath until fully solidified. Embedded samples were mounted on cryostubs and sectioned on a CryoStat (Thermo CryoStar NX70) equilibrated at -10.0 °C at 20.0 µm width, placed directly on sterile polysine adhesion microscopy slides (Thermo Scientific™ 10219280) and left to air dry in a fume cabinet overnight. Hybridisation was performed following the methodology described in the work of Gorham *et al*. (Gorham, Williams, Gidley, & Mikkelsen, 2016), with some adjustments, where 10.0 µL of hybridisation buffer (NaCl 5.0 M, Tris.HCl 1.0 M, formamide 25%, sodium dodecyl sulfate (SDS) 10%) was placed on top of each section, followed by the addition of 20 µL of each probe (Table 3), where the concentration of each probe was 50.0 ng μL^{-1}. Slides were placed in aluminium foil-wrapped 50.0-mL Corning® tubes and placed horizontally in an incubator set at 58.0 °C, and left overnight to hybridise. After hybridisation, the slides were recovered and washing buffer (NaCl 5.0 M, Tris.HCl 1.0 M, ethylenediaminetetraacetic acid (EDTA) 0.5 M, SDS 10%) was gently pipetted on top of each hydrogel section twice, followed by cold *dd*H_2O and leaving the slides to air dry in the dark. Prior to visualization, approximately 10.0 µL of Vectashield® anti-fade medium (VectorLabs, Maravai LifeSciences, Peterborough, UK) was gently pipetted on top of each resin, followed by placing a glass coversheet on top.

Table 3. List of fluorescent probe-tagged oligonucleotides for sequence-specific hybridisation with commensal bacteria in fermented starch matrices.

Probe name	Sequence (5' - 3')	Concentration (ng μL^{-1})	Storage Solution	Modification	Purchased From
Rbro730	TAAAGCCCAGYAGGCCG	50.0	Tris.HCl 10 mM, EDTA	5'-AF350	*Eurofins*

			1 mM, pH 8.1		
Bif164	CATCCGGCATTACCACCC	50.0	Tris.HCl 10 mM, EDTA 1 mM, pH 8.1	5'-ATTO740	*Eurofins*
Bac303	CCAATGTGGGGGACCTT	50.0	Tris.HCl 10 mM, EDTA 1 mM, pH 8.1	5'-RED	*Eurofins*
Eub338I	GCTGCCTCCCGTAGGAG	50.0	Tris.HCl 1 mM, EDTA 0.1 mM, pH 6.9	5'-CY5	*Eurofins*
Eub338II	GCAGCCACCCGTAGGTG	50.0	Tris.HCl 1 mM, EDTA 0.1 mM, pH 6.9	5'-CY5	*Eurofins*
Eub338III	GCTGCCACCCGTAGGTG	50.0	Tris.HCl 1 mM, EDTA 0.1 mM, pH 6.9	5'-CY5	*Eurofins*

2.8 Laser scanning confocal microscopy visualisation

Slides were visualised on a Zeiss LSM 880 Confocal Microscope, equipped with a fluorescent mercury lamp, equipped with diode (405 nm), Ar (458, 488, 514 nm), DPSS (561 nm) and He-Ne (594,633 nm) lasers for visualisation of AF350 (λ_{ex} = 350 nm), TxRed (λ_{ex} = 595 nm), CY5 (λ_{ex} = 645 nm) and ATTO740 (λ_{ex} = 743 nm) fluorescent tags. All images were taken under x10 (0.45, air) and x20 (0.8, air) magnification objectives, obtained and processed using the ZEN® Pro software package (Carl Zeiss Microscopy GmbH, Jena, Germany).

2.9 NMR spectroscopy

Solid-state ^{1}H-^{13}C cross-polarisation (CP) and cross-polarisation single pulse (CPSP) magic angle spinning (MAS) NMR experiments were carried out for the digested and fermented starch gels using a Bruker Avance III 400 MHz spectrometer, equipped with an HXY 4-mm probe, at a ^{13}C frequency of 100.64 MHz, and an MAS rate of 6.0 kHz. Gels were packed into inserts, closed with a stopper and a screw cap, and placed inside a 4-mm cylindrical rotor with a Kel-F end cap. The ^{1}H-^{13}C CP/MAS NMR experimental acquisition parameters were $\pi/2$ ^{1}H *rf* pulse of 3.30 µs and $\pi/2$ ^{13}C *rf* pulse of 3.40 µs, a contact time of 1000 µs, a recycle delay of 5 s, with a minimum of 7168 scans. ^{1}H and ^{13}C chemical shifts were referenced to tetramethylsilane (TMS). The spectra were measured at *ca*. 5.0 °C.

2.9.1 Estimation of mobility

Estimation of mobility levels across all ^{13}C sites was calculated using Equation 1 (Koev et al., 2020).

$$\%\, Mobility = \frac{I_{CPSP} - I_{CP}}{I_{CPSP}} \times 100 \qquad \textbf{\textit{Equation 1}}$$

where I_{CPSP} and I_{CP} are the ^{13}C peaks' normalised intensity values in their ^{1}H-^{13}C CPSP and CP/MAS NMR spectra, respectively.

2.9.2 Saturation transfer difference (STD) NMR spectroscopy

STD NMR experiments of all drug-loaded starch hydrogels were acquired using a Bruker Avance II 800 MHz spectrometer equipped with a triple resonance HR-MAS probe. Samples were spun at 6 kHz and experiments were carried out at 35 °C, using $\pi/2$ *rf* of 8.62 μs, and 64 scans. All STD experiments were performed using a pulse train of 50 ms shaped pulses for selective saturation of the starch matrix, using on- and off-resonance frequencies of 3.5 ppm and 50 ppm, respectively. Saturation times ranged from 0.1 to 10 s. A constant experiment length (saturation time + recycle delay) of 12 s was used.

To calculate the STD response (%), the peak intensities in the difference spectrum (STD_{OFF} - STD_{ON}, STD_{Δ}) were integrated relative to the peak intensities in the off-resonance (STD_{OFF}) (Gabrielli et al., 2021), according to the Equation 2.

$$STD\ (\%) = \frac{STD_{\Delta}}{STD_{OFF}} \times 100 \qquad \textbf{\textit{Equation 2}}$$

The rate of the STD (%) build-up is proportional to the intermolecular distance between the guest and the host molecule, as the rate of saturation transfer by means of intermolecular nuclear Overhauser effect (nOe) is distance-dependent.

2.10 Branching analyses

The branching analysis was performed as described in (Tizzotti, Sweedman, Tang, Schaefer, & Gilbert, 2011). Starch hydrogels sampled at the end of the INFOGEST simulated digestion treatment and after 24, 48 and 72 h of *in vitro* fermentation were flash frozen in liquid N_2, lyophilised (Thermo ModuLyod freeze drier) for 3 days, manually ground using mortar and pestle, and dissolved in DMSO-d_6 (containing LiBr 0.5% w/v) at a concentration of 2.85 mg mL^{-1}. Samples were vortex-mixed for 10 s, followed by the addition of 600-μL aliquots of the solutions directly into NMR tubes (Norell® Select Series™, 5 mm). A single drop of TFA-d_1 was added to each NMR tube immediately prior to spectral acquisition using a Pasteur pipette. The NMR experiments were performed on a Bruker Avance II NMR spectrometer, operating at a ^{1}H frequency of 500.11 MHz, equipped with an inverse triple resonance z-gradient probe. The acquisition parameters were $\pi/2$ *rf* pulse on ^{1}H of 10 s, recycle delay of 12 s, acquisition time of 3.2 s, and 128 scans. All experiments were performed in triplicate. The degree of branching was determined as the percentage of the integration of the peak at 4.78 ppm, out of the combined proportion of the peaks at 5.10 and 4.78 ppm, associated with α(1-4) and α(1-6) glycosidic linkages, respectively.

2.11 Bacterial metabolite and small molecule release quantification

The samples containing the supernatant from the fermentation media were thawed out, centrifuged (3,000 x g for 3 min) and 400 µL aliquots were pipetted directly into NMR tubes (Norell® Standard Series™, 5 mm), followed by the addition of 200 µL of phosphate buffer (NaH_2PO_4 (21.7 mM), K_2HPO_4 (82.7 mM), NaN_3 (8.6 mM), 3-(trimethylsilyl)-propionate-d_4 (TMSP, 1.0 mM)) (Vignoli et al., 2019). The spectra were recorded on a Bruker Avance III 800 MHz spectrometer, equipped with an inverse triple resonance z-gradient probe. All ^{1}H NMR spectra acquired on the 800 MHz spectrometer were obtained using 256 scans, a spectral width of 9615 Hz, acquisition time of 0.83 s, using Bruker's '*noesygppr1d*' pulse sequence, featuring selective low-power pre-saturation (p16 = 1.0 ms) on the residual H_2O peak frequency during relaxation delay and mixing time for effective solvent suppression. Spectra were apodised using 0.1 Hz line broadening and referenced using the TMSP peak (0.0 ppm). Recycle delay was set to 10 s, the mixing time used was 0.1 s, and the ^{1}H $\pi/2$ *rf* pulse was 9.08 µs. The metabolites were quantified using the NMR Suite v7.6 Profiler (Chenomx®, Edmonton, Canada).

The small molecular release in the fermentation media was quantified against the TMSP reference, using the acquisition parameters above, against distinct ^{1}H peaks of the three small molecules (9.6 ppm for VNL, 7.7 ppm for 5FU, and 1.1 pm for DOX) on the basis of standard curves of known concentrations of small molecules in phosphate buffer (*see above*).

2.12 Dynamic oscillatory rheology

The undigested, digested and fermented hydrogels' response to external stress was analysed following a previously described protocol (Koev et al., 2020), with the modification of all samples being analysed at a constant temperature of 37 °C.

2.13 Size-exclusion chromatography (SEC)

Undigested, digested, and fermented hydrogel samples intended for SEC and fluorophore-assisted carbohydrate electrophoresis (FACE) were flash frozen under liquid N_2 and lyophilised for 5 days, followed by manual grinding using a mortar and pestle. Samples for debranched SEC and FACE were debranched following Wu *et al.*(Wu, Li, & Gilbert, 2014)

The molecular structural parameters of whole starch molecules in the hydrogels were characterised using an Agilent 1100 series SEC system (Agilent Technologies, Santa Clara, CA) equipped with a Shimadzu RID-10A differential refractive index detector (Shimadzu Corporation, Kyoto, Japan). Fully branched samples were run using GRAM 30 and GRAM 3000 columns (Polymer Standards Service (PSS), GmbH, Mainz, Germany) connected sequentially, providing separation in the range of 5_X10^3 – 5_X10^6 Da (R_h of 0.5 – 50.0 nm), whereas debranched samples were analysed using GRAM 30 and GRAM 1000 columns, appropriate for separation in the range of 100 – 10^6 Da. All samples were run at 80.0 °C, using dimethyl sulfoxide (DMSO, 99.5% w/w) and LiBr (0.5% w/w) as the mobile phase, at a flow rate of 0.3 and 0.6 mL min^{-1} for branched and debranched samples, respectively. The mobile phase was

prepared by dissolving LiBr (0.5% w/w) in DMSO under sonication for 1 h, followed by filtration under pressure (45.0 μm, PTFE membrane). All samples were dissolved in the eluent at a concentration of 2.0 mg mL^{-1} and placed in a thermomixer (Eppendorf thermomixer C), set at 100 r.p.m., at 80 °C for 5 h. This was followed by loading the samples directly in SEC vials for analysis. Under these conditions, the elution time of the branched polymers is dependent on its hydrodynamic volume, V_h (where $V_h = 4/3_X\pi R_h^3$), using a series of pullulan standards (PSS, GmbH, Mainz, Germany) in the range of 180 Da – 1.2_X10^6 Da for calibration, using the methods described in Li *et al*. (Li, Prakash, Nicholson, Fitzgerald, & Gilbert, 2016) Elution time was converted to R_h, and (for debranched samples) from R_h – to the degree of polymerization (DP) X, using the Mark-Houwink relation (Vilaplana & Gilbert, 2010), giving X (R_h).

2.14 Fluorophore-assisted carbohydrate electrophoresis (FACE)

The debranched samples intended for FACE analysis were labelled using 8-aminopyrene-1,3,6-trisulfonate (APTS, Carbohydrate Labelling and Analysis Kit, Beckman Coulter, Brea, CA, USA) according to Wu *et al*.(Wu et al., 2014) The samples were analysed on a PA-800 Plus FACE System (Beckman-Coulter, Brea, CA, USA), coupled with a solid-state laser-induced fluorescence (LIF) detector and an argon-ion laser as the excitation source. The separation was carried out in an N-CHO-coated capillary (50.0-μm in diameter, Carbohydrate Labelling and Analysis Kit). The sample was introduced into the capillary in a carbohydrate separation buffer (Beckman-Coulter, 477623) by pressure injection for 3.0 s at 0.5 psi. Separation of the labelled linear glucans was achieved using an applied voltage of 28–30.0 kV (≈14.0 mA) at 25.0 °C, where the first ≈120 peaks were separated over a total time of 60 min. Under these conditions, the chain length distribution (CLD) of all debranched samples was analysed and presented as percentile contribution of each DP to the total CLD, where DP is the number-average degree of polymerisation. min. Elution time was converted to R_h, and (for debranched samples) from R_h – to the degree of polymerization (DP) X, using the Mark-Houwink relation (Vilaplana & Gilbert, 2010), giving X (R_h).

2.15 Participant information & ethics

Faecal sample was obtained from four adult (≥ 18 years old), free-living, healthy donors who had not taken antibiotics in the 3 months prior to donation, and were free from gastrointestinal disease. Ethical approval was granted by Human Research Governance Committee at the Quadram Institute (IFR01/2015) and London - Westminster Research Ethics Committee (15/LO/2169) and the trial was registered on clinicaltrials.gov (NCT02653001). A signed informed consent was obtained from the participant prior to donation.

2.16 Statistical analyses

The statistical significance of the changes in degree of branching following *in vitro* digestion and fermentation, as well as the changes in the concentration of bacterial metabolites in the presence of the three guest molecules – vanillin, 5-fluorouracil and doxorubicin compared to the controls, were assessed using a 2-way analysis of variance (ANOVA)

with Tukey's multiple comparisons test with a 95% confidence interval, using GraphPad Prism 9.0.0 (GraphPad Software, Inc.) statistical software.

3. Results & discussion

3.1 Starch hydrogel bulk properties & molecular organisation through the GIT

The impact of amylose content on starch' physicochemical properties and susceptibility to amylolytic degradation has been well documented in the literature (Fredriksson, Silverio, Andersson, Eliasson, & Åman, 1998; Gong, Cheng, Gilbert, & Li, 2019a; Koev et al., 2020; Tao, Li, Yu, Gilbert, & Li, 2019). In order to probe the viability of NM and H7 starch gels as drug delivery vehicles for targeted release in the distal parts of the GIT, it is important to investigate the structural changes occurring in the hydrogel structure and organisation. Parameters, such as chain length distribution, degree of branching, and overall matrix structural integrity all have an important impact on polymer-based pharmaceutical excipients' disintegration and drug dissolution profiles.

Both NM and H7 starch hydrogels exhibited progressive decrease in their storage moduli as they traverse the length of the simulated GIT. NM hydrogels lose structural stability faster, compared to H7 ones, evidenced by NM's significant drop in storage moduli occurring between 12 and 24 h of fermentation, whereas this happens later for H7 gels (between 24 and 48 h of fermentation, figures S1-3, Supplementary data). This delay in loss of structural integrity is likely a result of NM's higher susceptibility to enzymatic degradation, compared to H7 (Figure S4, Supplementary data). The progressive decrease in the % strain at the substrates' breaking point as they traverse the GIT (Figure S3, Supplementary data), is likely to have an impact on their role as pharmaceutical excipients by way of influencing their rate of disintegration and drug release throughout the GIT.

The molecular size distributions of both branched and debranched gels at successive stages in the simulated GIT (Figures S5-10, Supplementary data) revealed differences in the molecular structural parameters (hydrodynamic radius, R_h; and degree of polymerisation, DP) between NM and H7 starch hydrogels. The amylopectin fraction ($R_h \approx 200$ nm, Figure S9, Supplementary data, Tao et al., 2019) in whole NM gels exhibited a greater susceptibility to upper GIT amylolytic digestion, compared to H7's (Figure S9, UD *vs* D2, Supplementary data), as seen in earlier works (Witt, Gidley, & Gilbert, 2010). Unlike previous works probing the amylolytic susceptibility of lyophilised gelatinised starch (Gong, Cheng, Gilbert, & Li, 2019b; Witt et al., 2010), our data showed minimal changes occurring in the upper GIT in the molecular structural parameters of H7 hydrogels (Fig. S9, UD *vs* D2, Supplementary data), highlighting the impact of the macromolecular hydrogel organisation and structure on its susceptibility to α-amylase digestion and the accessibility of the enzyme to the substrate (Dhital et al., 2017). This provides further context for the digestibility and rheological data, indicating it is the amylopectin fraction's greater susceptibility to α-amylase degradation that has a greater impact on the hydrogels' gradual loss of structural integrity in the upper GIT, compared to amylose.

The size distributions of the debranched NM and H7 gels revealed some decrease in the contribution of longer amylose chains (DP ≈ 1000 – 7000, UD *vs* D2, Figure S10, Supplementary data), accompanied by a slight increase in the contribution of shorter chains (DP ≈ 10 – 50, UD *vs* D2, Figure S10, Supplementary data). This increase in shorter chains was also evidenced in the hydrogels' parametrised chain lengths (Figures. S11-14, Supplementary data) (Hanashiro, Abe, & Hizukuri, 1996). There was a small population of amylose chains (DP ≈ 1000-1100, Figure S10, Supplementary data), which was still present after *in vitro* digestion and fermentation, likely to be linked to an increased structural stability, and lower susceptibility to enzymatic degradation of this linear polymer fraction (Clark, Gidley, Richardson, & Ross-murphy, 1989).

In both the branched and debranched size distributions, the most pronounced changes in the hydrogels' molecular structural parameters occurred during the fermentation stages in the simulated colon (Figures S9-10, UD *vs* F72, Supplementary data). These are likely to be the result of the cumulative action of multiple hydrolytic enzymes featuring both α(1-4) and α(1-6) specificity, unlike across the upper GIT where starch gels are exposed exclusively to α(1-4) hydrolytic enzymes (salivary and pancreatic α-amylase) (Butterworth, Warren, & Ellis, 2011; Flint et al., 2012; Kaoutari et al., 2013). This is further supported by the preferential cleavage of α(1-4) linkages during the upper GIT digestion stages, followed by preferential cleavage of α(1-6) glycosidic bonds in the large intestinal phase, shown by ^{1}H NMR (Fig. S16, Supplementary data).

3.2 Starch hydrogel internal mobility

We probed the change in the degree of local mobility across all ^{13}C environments in NM and H7 starch hydrogels as they traverse the entire length of the simulated GIT. There was a progressive increase in degree of mobility of solvated chains across all ^{13}C sites with each successive digestion and fermentation stage, accompanied by a simultaneous progressive decrease in their G' (kPa) and strain (%) values at their cross-over point (*i.e.,* point of loss of structural integrity, Figure 1).

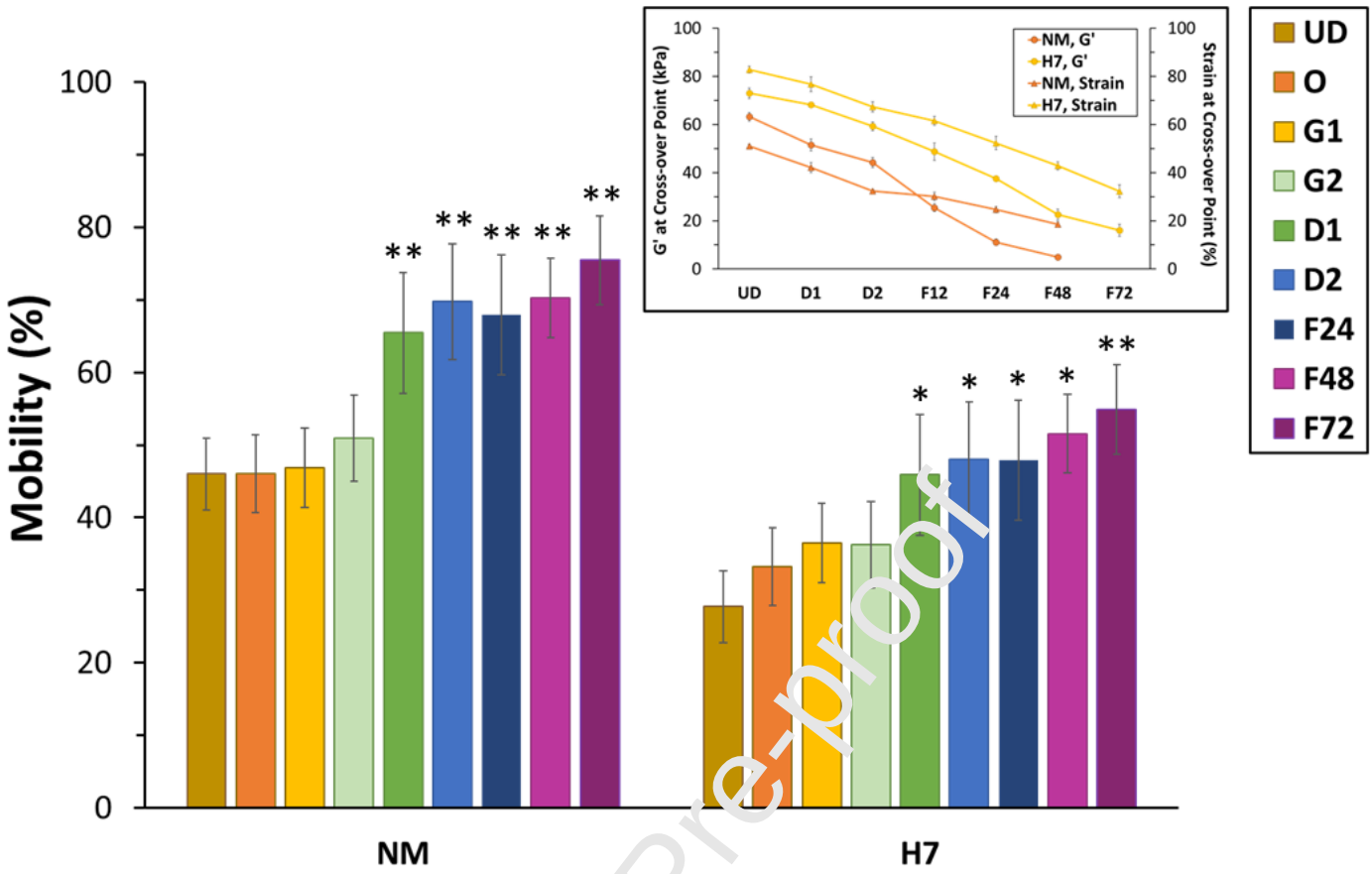

Figure 1. Estimated levels of local mobility averaged across all ^{13}C environments in normal maize (NM) and Hylon VII® (H7) starch hydrogels before digestion (UD), at various INFOGEST digestion (O, G1, G2, D1, D2) and *in vitro* fermentation stages (F24, F48 and F72). Inlay showing cross-over point analysis of NM and H7 gels before and during INFOGEST digestion, and during *in vitro* fermentation, featuring the samples' G' (kPa) and strain (%) values at their respective G cross-over points. Error bars are based on the standard deviation across a minimum of three replicates, where * $p<0.05$, ** $p<0.005$.

Solid-state NMR spectra (^{1}H-^{13}C CP and CPSP/MAS) of the starch hydrogels at the end of simulated digestion (Figure 2, NM, D2, and Figure S15, Supplementary data) revealed the presence of new sharp peaks in the CPSP spectrum at *ca*. 93 and 96 ppm, the chemical shift of which overlapped with peaks in the solution state NMR spectrum of the digesta at the end of simulated INFOGEST protocol (Figure 2, Digesta). Comparison of the ^{1}H-^{13}C CPSP/MAS spectrum of the starch gels at the end of *in vitro* digestion, as well as the solution state NMR spectrum of the digesta with the solution-state spectrum of an equimolar (1.0 mM) mixture of reducing sugars (Figure 2, glucose, maltose, maltotriose), revealed the identity of the newly observed sharp peaks to be solvated products of digestion (DP ≈ 1 – 3) remaining trapped inside the water-filled pores of the starch hydrogels, as well as in the digesta following simulated upper GIT enzymatic hydrolysis.

The newly observed peaks assigned to a combination of reducing sugars. *i.e.*, glucose, maltose and maltotriose, were no longer present after 24 h of *in vitro* fermentation (Figure 2, F24). This is likely to be a consequence of their easier utilisation as a carbon source by commensal bacteria (Barrangou et al., 2006; Durica-Mitic, Göpel, & Görke, 2018), compared to the pre-digested starch matrix.

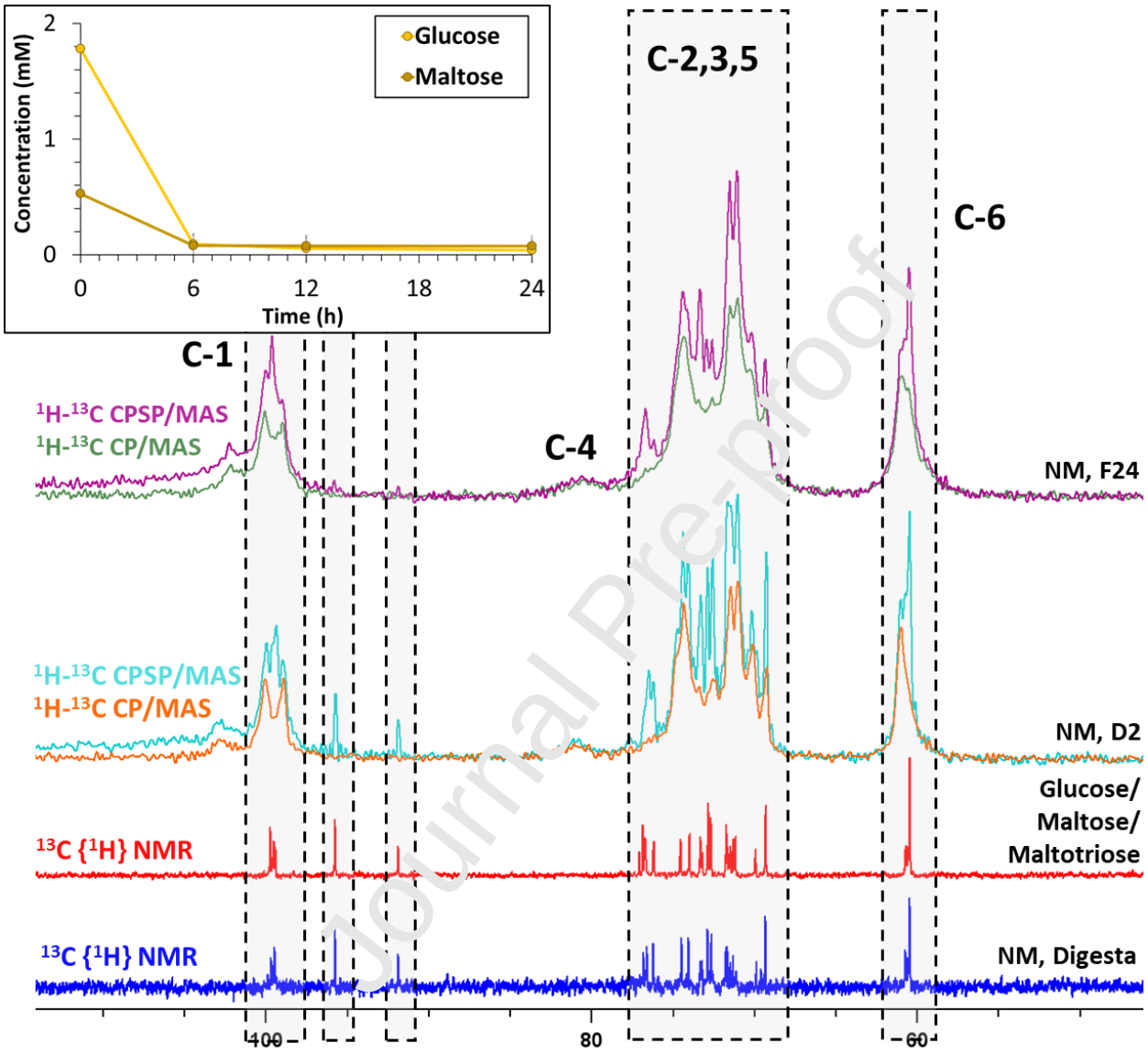

Figure 2. ^{1}H-^{13}C CP and CPSP MAS NMR spectra (orange and green, and cyan and magenta, respectively) of normal maize (NM) starch hydrogels at the end of INFOGEST digestion (D2), and after 24 h of *in vitro* fermentation (F24), direct detection ^{13}C{^{1}H} solution state NMR of glucose, maltose and maltotriose (1.0 mM in D_2O each, red), and of the digesta at the end of INFOGEST digestion (blue). Inlay showing changes in concentration of glucose and maltose (yellow and brown, respectively) across 72 h of *in vitro* fermentation of both NM substrates (circles).

3.3 Starch hydrogels' viability as targeted colonic drug delivery platforms

Across all samples, the drug release was confined to the large intestine with minimal to no release in the upper GIT (Figure 3). The drug molecules' release rates were several times lower than other starch-based nanoparticle and polysaccharide hydrogel-type colonic drug delivery platforms of polysaccharide origin (Bisharat et al., 2019; Vashist, Vashist, Gupta, & Ahmad, 2014) (*e.g.*, 70-100% drug released from other nanoparticles and gels after 24 h vs 15-56% from NM and H7 hydrogels, Figure 4) (Bisharat et al., 2019; Chaichi, Hashemi, Badii, & Mohammadi, 2017; Jacobs, D.M., Deltimple, N., van Velzen, E., van Dorsten, F.A., Bingham, M., Vaughan, E.E., van Duynhoven, 2008; Phan et al., 2021; Sintov, Di-Capua, & Rubinstein, 1995; Vashist et al., 2014). This prolonged drug release stage is likely to play an important role in patients with colorectal pathologies, such as irritable bowel disease (IBD) and irritable bowel syndrome (IBS), and those with increased colonic epithelial surface area (e.g., colorectal polyps), whose colonic transit times can be on the scale of days (Asnicar et al., 2021; Muhammad, Lamendola, Daas, Kumar, & Vidyarthi, 2014). These data highlight starch hydrogels' superiority as targeted colonic drug delivery vehicles with prolonged release, allowing for longer therapeutic windows and lower frequency of drug administration – two important parameters in patients' quality of life. Unlike traditional colonic pharmaceutical excipients, exhibiting sigmoidal release kinetics with rapid release of the guest molecule (Rujivipat & Bodmeier, 2010a; Tu et al., 2010), these starch hydrogels show a more gradual pharmacokinetic release profile (1.25-3% vs 0.63-2.1% drug release per hour, respectively) (Bisharat et al., 2019; Phan et al., 2021).

Drug carriers' structural integrity has a significant impact on their role as excipients, as well as on the pharmacokinetic profile of the loaded drug molecules (Peppas et al., 2000). The drug release kinetics mimic the trends observed in the loss of the excipients' structural integrity (Figure 3, inlay). H7's delayed degradation across the entire length of the GIT compared to NM was mirrored by the two hydrogels' pharmacokinetic profiles when loaded with the three guest molecules (Figure 3), where all three drugs were consistently released faster from the NM gels compares to the H7 gels. These data show it is matrix disintegration that appears to be the dominating factor in the pharmacokinetic profile of the loaded drug molecules across the GIT.

Each of the three guest molecules showed different release kinetics, with VNL showing the most rapid release kinetics in the *in vitro* colonic phase, followed by DOX and 5FU (Figure 3). Differences in release kinetics may be influenced by the small molecules' different degree of proximity and interaction with the starch backbone, where the distance between the drug and the host followed the order of VNL < DOX < 5FU, with interaction strengths estimated by STD NMR (Figures S17-S19, Supplementary data). The more spatially distal (and more loosely associated with the starch backbone) small molecules showed the most rapid release kinetics, with the more spatially proximal to the starch backbone being released more slowly and less completely. In our previous work we showed there were no significant differences in the interaction between the starch backbone and the water molecules in starch hydrogels, as probed by water polarisation transfer-cross-polarisation (WPT-CP) and STD NMR (Koev et al., 2020). Furthermore, there was no correlation between the hydrophilicity of the three guest molecules (logP VNL = 121; logP 5FU = -0.66; logP DOX =

127) and their respective drug release profile. These data suggest any differences in the pharmacokinetic profile of the three small drug molecules are likely to be the result of multiple factors influencing the guest-host hydrogel systems.

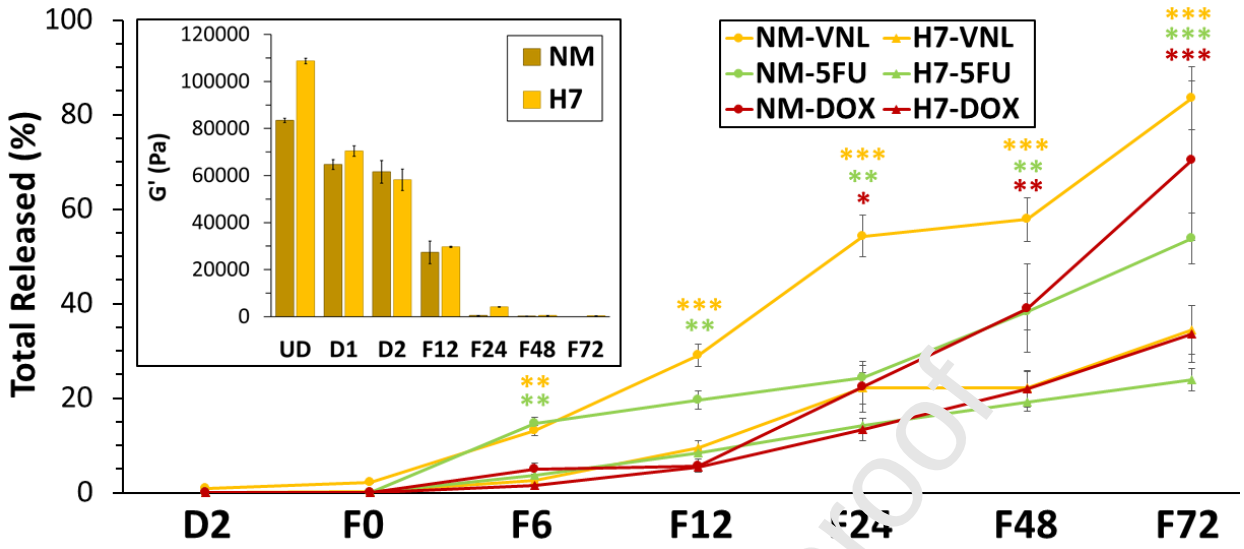

Figure 3. Release profiles of 5FU, VNL and DOX from normal maize (NM) and Hylon VII® (H7) starch hydrogels during the end of the *in vitro* digestion (D2) and fermentation experiments (F0-72). Inlay showing progressive changes in G' (Pa) of NM and H7 hydrogels before (UD), during *in vitro* digestion (D1 and D2), and fermentation (F12-72). Error bars are based on the standard deviation across a minimum of three replicates. Statistical significance symbols (*) refer to significant differences in the release kinetics between NM and H7 at a given time point (VNL – yellow, 5FU – green, DOX – red), where * ($p<0.05$), ** ($p<0.01$) and *** ($p<0.001$).

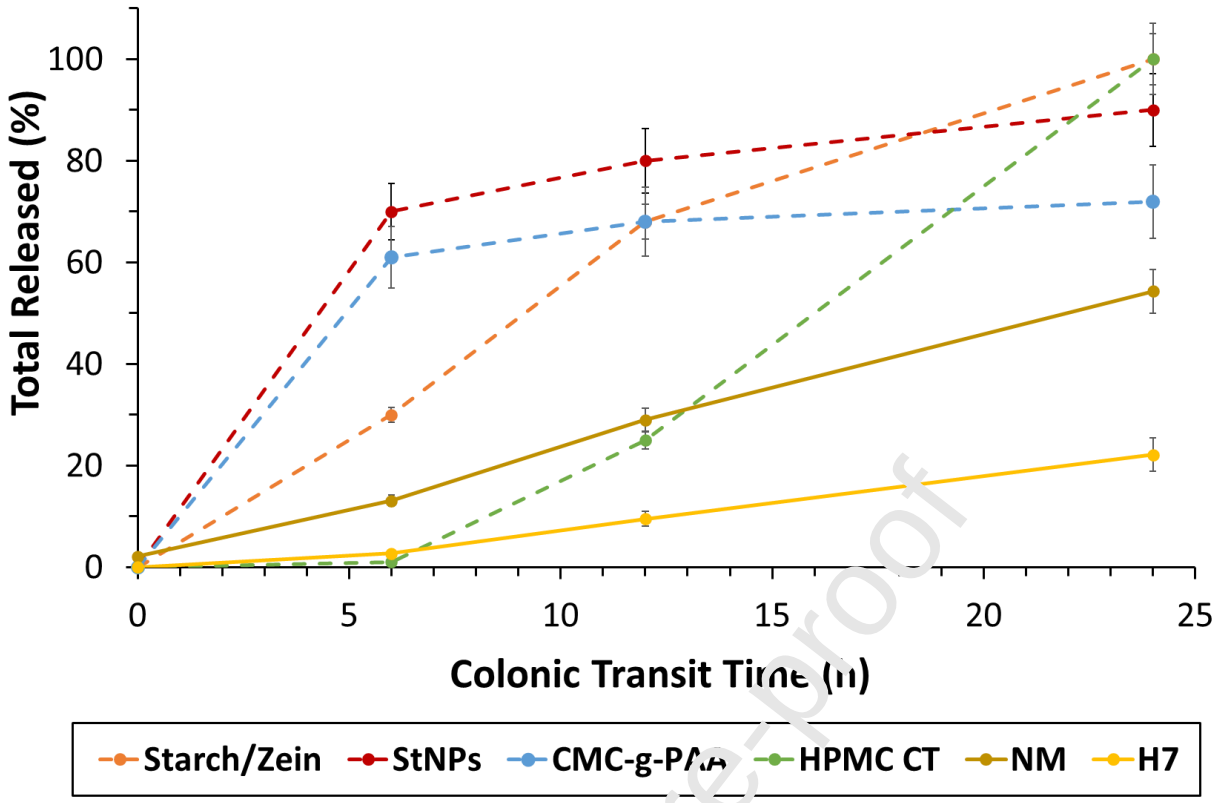

Figure 4: Comparative colonic drug release kinetics between VNL-loaded normal maize (NM) and Hylon VII® (H7) starch hydrogels, and four competitor drug delivery platforms: starch/zein films (Bisharat et al., 2019), amphiphilic starch nanoparticles (StNPs) (Phan et al., 2021), carboxymethylchitosan-g-polylactic acid (CMC-g-PAA) (Tu et al., 2010), and hydroxypropyl methylcellulose compression tablets (HPMC CT) (Rujivipat & Bodmeier, 2010b).

One of the advantages of applying starch hydrogels (*i.e.*, RS III) as pharmaceutical excipients is their health-promoting auxiliary properties, such as their fermentability by commensal bacteria, resulting in the production of physiologically relevant bacterial metabolites (*e.g.*, SCFAs), which have been linked with a range of health benefits (Birt et al., 2013; Cotter et al., 2015; Cryan & O'Mahony, 2011). Across all participants, NM starch hydrogels led to the production of more SCFAs, compared to H7, where the ratio between acetate, propionate and butyrate was 50:25:25 for NM, and closer to 60:20:20 for the H7 starch gels (Figure 5), similar to previous works (Den Besten et al., 2013). Despite the overall comparable concentration of SCFAs produced from the two starch hydrogel types, the more digestible NM substrate led to the production of more than threefold more gas compared to H7 (Figure S20, Supplementary data). Cumulatively these data show that the more digestible low-amylose NM hydrogel substrate is also more fermentable in the colon. These observations are in line with previous data on the fermentation profile of various resistant starches and non-starch polysaccharides in the colon (Wang, Zhu, Li, Wang, & Jensen, 2004).

There were no significant differences in the concentrations of acetate, butyrate, lactate, and succinate in the presence of VNL, 5FU and DOX, compared to the controls, across all NM and H7 starch hydrogels. The only significant differences observed were the increased production of propionate in the presence of 5FU in both hydrogel excipients (Figures S21 and S22, Supplementary data). These data indicate starch hydrogels are able to provide targeted release of orally administrable drug molecules to the colon, without significantly perturbing commensal bacterial SCFA metabolic pathways.

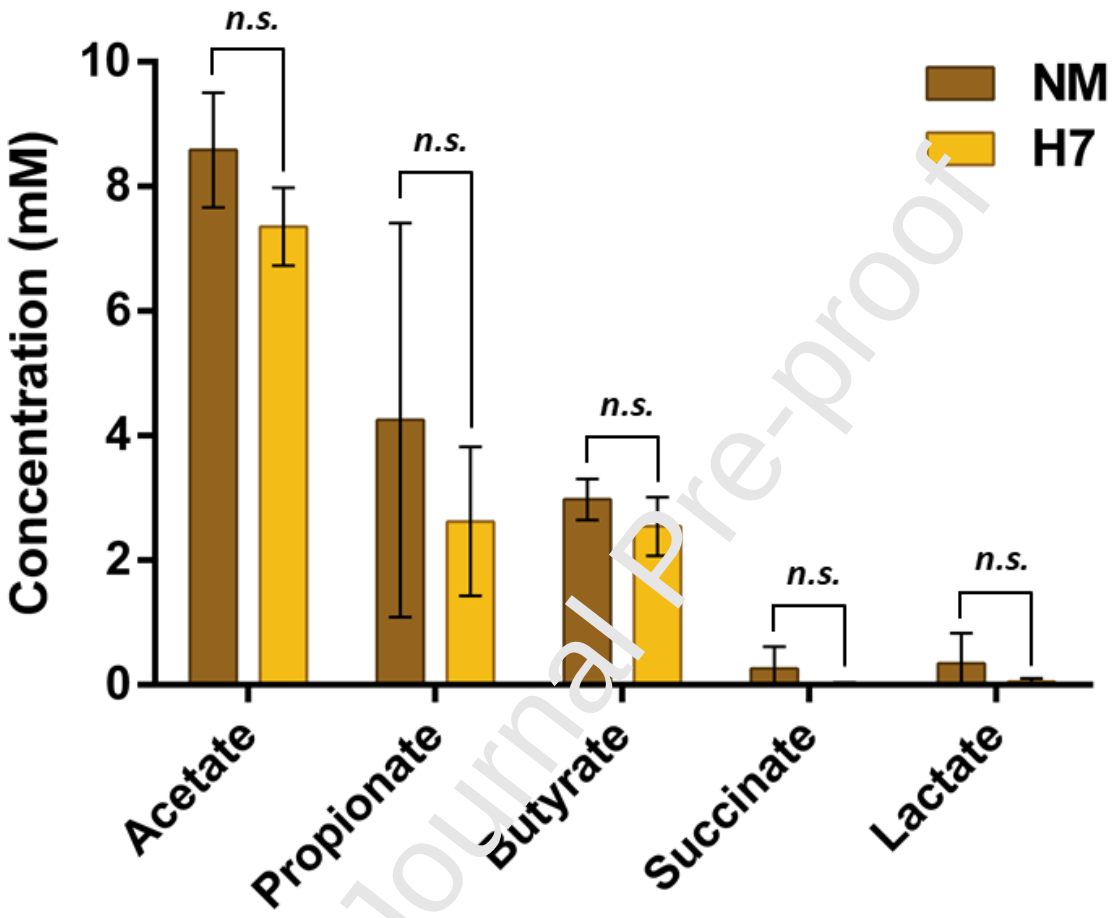

Figure 5. Cumulative concentration of SCFAs over 72 h of *in vitro* fermentation of normal maize (NM) and Hylon VII® (H7) starch hydrogels by bacteria from human faecal donors. All measurements presented are averaged out across 4 different individuals with a minimum of 3 replicates per individual. Error bars are based on the standard deviation between measurements across all samples, where n.s. denotes lack of statistical significance.

3.4 Commensal bacteria's interaction with starch hydrogels

An aspect often neglected in the context of colonic pharmaceutical excipients, is their interaction with the commensal microflora, and the consequences of this interplay on the drug delivery vehicle's stability and the pharmacokinetic profile of the drug molecules (Bisharat et al., 2019).

FISH staining viewed with LSCM revealed differences in how bacteria interact with NM and H7 starch hydrogels – both in the localisation of bacterial colonies, and in the rate of colonisation of the starch matrix. Unlike *R.bromii* and *Bacteroides*, which do not appear to cluster in larger groups, but rather invade the starch gel matrices in smaller, individualised colonies, *Bifidobacteria* appear to concentrate along the periphery and surface of the gel matrix (Figure 6). This could be a result of the cooperative nature of *Bifidobacterium* communities (Callaghan & Sinderen, 2016; Lawson et al., 2019).

The colonisation appears to be time-dependent, irrespective of bacterial species and starch type, where there are fewer commensal bacterial colonies at earlier fermentation times (6 – 24 h), compared to later ones (48 – 72 h, Figure 6). In all cases, the colonisation appears to be from the periphery inwards, with *R.bromii* and *Bacteroides* exhibiting a greater rate of colonisation of the matrices, compared to *Bifidobacteria*, and the rate of commensal bacterial invasion into the matrix being greater in NM than in H7 (Figures S23-26, Supplementary data). This could be a direct result of the distinctly different morphology of the two gels before and during the different stages of *in vitro* fermentation, where H7 appears as a uniform, cohesive matrix with little-to-no pores or channels throughout its surface, whereas NM hydrogels appear to have numerous channels and "cracks" along their surface. These surface channels are likely to be responsible for the easier accessibility and greater rate of bacterial colonisation of NM starch hydrogels during *in vitro* fermentation. Both hydrogel samples undergo visible changes in their morphology as a function of time during the process of *in vitro* fermentation, which is exhibited as the gradual formation of pores and channels in the hydrogel surface, with the diameter of those increasing towards the later stages of fermentation, where in the case of NM gels, these reach sizes greater than 100 μm (Figure S24, Supplementary data). These differences in the formation of internal cavities are also likely to play a role in the loss of bulk structural integrity of the two starch hydrogels (Figures S1-3, Supplementary data).

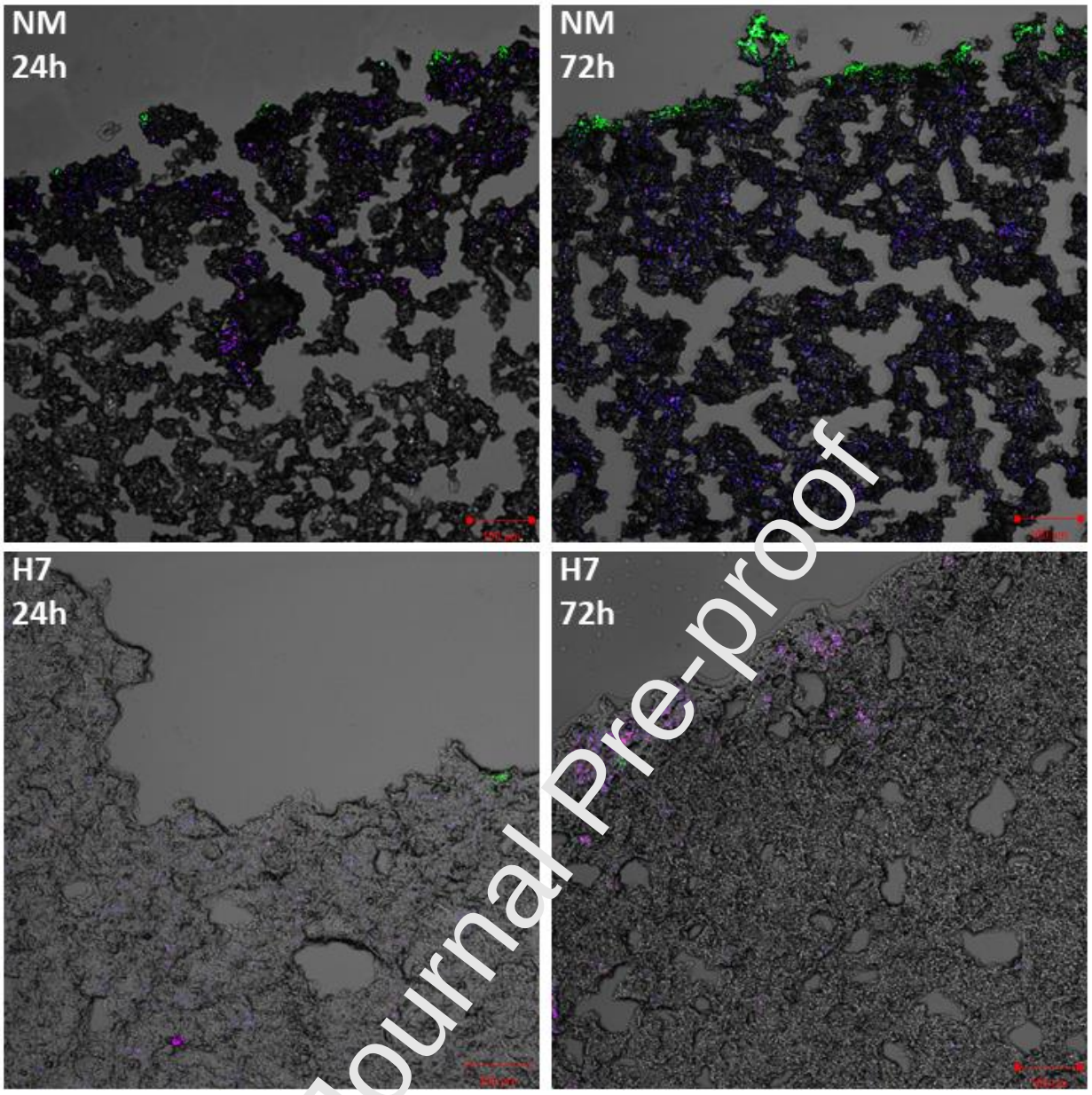

Figure 6. Peripheral image of normal maize (NM) and Hylon VII® (H7) starch hydrogels after 24 h (NM 24h and H7 24h) and after 72 h (NM 72h and H7 72h) of *in vitro* fermentation, visualised by LSCM at 10x magnification, with the hydrogel morphology and all three bacterial probes: *R.bromii* (blue), *Bacteroides* (red) and *Bifidobacterium* (green). Scale bar set at 100 μm.

On addition of non-specific bacterial probes (Eub338I, Eub338II and Eub338III, Table 3) probes to the combination of *R.bromii*-, *Bacteroides*- and *Bifidobacteria*-specific probes, it was revealed that the combination of the three specific probes accounts for a high proportion (62 – 76%) of the bacteria colonising the starch hydrogel matrices during fermentation (Figures S27-30, Supplementary data). Once again, an accumulation of bacterial species was observed

around the periphery of the gels, where this proportion was greater in the non-specific bacterial species, compared to the *Bifidobacteria*, likely linked to the colony-forming behaviour of other commensal bacterial species.

4. Conclusions

In this study we have systematically quantified the extent of bulk and molecular level structural changes low- and high-amylose starch hydrogels undergo at each stage of the human GIT, using two widely accepted models of *in vitro* digestion and colonic fermentation. This approach has the advantage of being a more adequate representation of the human GI conditions pharmaceutical excipients are exposed to, compared to United States and British Pharmacopoeia (USP and BSP, respectively) utilised methods, which can omit the use of hydrolytic enzymes, or exclusively focus on one part of the GIT. This work systematically probes the structure-function links underpinning starch gels' role as pharmaceutical excipients at each individual stage of the human GIT. We link structural parameters defining starch hydrogels' macromolecular organisation, with molecular mobility of internally solvated starch chains, and show how these dictate gels' rate of hydrolysis across the GIT. The viability of starch hydrogels as orally administrable drug delivery platforms for targeted release of drug molecules in the colon has been demonstrated. It has been shown how one can modulate their choice of starch to achieve a highly tuned pharmacokinetic profile in the colon. Furthermore, we have demonstrated the ability of commensal bacteria to degrade starch hydrogels, leading to the production of health-promoting metabolites, such as SCFAs. These findings provide important insight for the application driven design of novel drug delivery platforms for targeted drug release in distal parts of the human GIT.

CRediT Authorship Contribution Statement

TTK – Conceptualisation, Data curation, Formal analysis, Investigation, Methodology, Writing – original draft, review & editing.

HCH – Methodology, Writing – review & editing.

SK – Data curation.

YZK – Conceptualisation, Methodology, Supervision, Writing – review and editing.

FJW – Conceptualisation, Formal analysis, Funding acquisition, Methodology, Supervision, Writing – review & editing.

Conflicts of Interest

There are no conflicts to declare.

Acknowledgements

The authors are grateful for Professor Robert 'Bob' Gilbert's access to size-exclusion chromatographic equipment at the agricultural college of YangZhou university, Jiangsu Province, China. TTK, HCH, FJW and YZK would like to acknowledge the support of a Norwich Research Park Science Links Seed Fund. FJW, HCH and TK gratefully acknowledge the support of the Biotechnology and Biological Sciences Research Council (BBSRC); this research was funded by the BBSRC Institute Strategic Programme Food Innovation and Health BB/R012512/1 and its constituent projects BBS/E/F/000PR10343 and BBS/E/F/000PR10346. The Engineering and Physical Sciences Research Council (EPSRC) is acknowledged for provision of financial support (EP/N033337/1) for Y.Z.K. TK would like to thank the Quadram Institute for funding his PhD Scholarship. We are also grateful to UEA Faculty of Science NMR facility.

Notes

Supporting information includes INFOGEST protocol, batch colon model protocol, rheology, digestibility, SEC, branching analysis, STD NMR, SCFAs production data, and confocal microscopy data.

References

Ali, A. E., & Alarifi, A. (2009). Characterization and *in vitro* evaluation of starch based hydrogels as carriers for colon specific drug delivery systems. *Carbohydrate Polymers*, *78*(4), 725–730. https://doi.org/10.1016/j.carbpol.2009.06.009

Amidon, S., Brown, J. E., & Dave, V. S. (2015). Colon-targeted oral drug delivery systems: design trends and approaches. *AAPS PharmSciTech*, *16*(4), 731–741. https://doi.org/10.1208/s12249-015-0350-9

Asnicar, F., Leeming, E. R., Dimidi, E., Mazidi, M., Franks, P. W., Al Khatib, H., … Berry, S. E. (2021). Blue poo: Impact of gut transit time on the gut microbiome using a novel marker. *Gut*, *70*(9), 1665–1674. https://doi.org/10.1136/gutjnl-2020-323877

Bagliotti Meneguin, A., Stringhetti Ferreira Cury, B., & Evangelista, R. C. (2014). Films from resistant starch-pectin dispersions intended for colonic drug delivery. *Carbohydrate Polymers*, *99*, 140–149. https://doi.org/10.1016/j.carbpol.2013.07.077

Barrangou, R., Azcarate-Peril, M. A., Duong, T., Conners, S. B., Kelly, R. M., & Klaenhammer, T. R. (2006). Global analysis of carbohydrate utilization by *Lactobacillus acidophilus* using cDNA microarrays. *Proceedings of the National Academy of Sciences of the United States of America*, *103*(10), 3816–3821. https://doi.org/10.1073/pnas.0511287103

Birt, D. F., Boylston, T., Hendrich, S., Jane, J.-L., Hollis, J., Li, L., … Whitley, E. M. (2013). Resistant starch: Promise for improving human health. *Advances in Nutrition*, *4*(6), 587–601. https://doi.org/10.3945/an.113.004325

Bisharat, L., Barker, S. A., Narbad, A., & Craig, D. Q. M. (2019). *In vitro* drug release from acetylated high amylose

starch-zein films for oral colon-specific drug delivery. *International Journal of Pharmaceutics*, *556*(October 2018), 311–319. https://doi.org/10.1016/j.ijpharm.2018.12.021

Brodkorb, A., Egger, L., Alminger, M., Alvito, P., Assunção, R., Ballance, S., … Recio, I. (2019). INFOGEST static *in vitro* simulation of gastrointestinal food digestion. *Nature Protocols*, *14*(April), 991–1014.

Butterworth, P. J., Warren, F. J., & Ellis, P. R. (2011). Human α-amylase and starch digestion: An interesting marriage. *Starch/Staerke*, *63*(7), 395–405. https://doi.org/10.1002/star.201000150

Callaghan, A. O., & Sinderen, D. Van. (2016). Bifidobacteria and their role as members of the human gut microbiota. *Frontiers In*, *7*(June). https://doi.org/10.3389/fmicb.2016.00925

Cerf-Bensussan, N., & Gaboriau-Routhiau, V. (2010). The immune system and the gut microbiota: Friends or foes? *Nature Reviews Immunology*, *10*(10), 735–744. https://doi.org/10.1038/nri2850

Chaichi, M., Hashemi, M., Badii, F., & Mohammadi, A. (2017). Preparation and characterization of a novel bionanocomposite edible film based on pectin and crystalline nanocellulose. *Carbohydrate Polymers*, *157*, 167–175. https://doi.org/10.1016/j.carbpol.2016.09.062

Clark, A. H., Gidley, M. J., Richardson, R. K., & Ross-murphy, S. B. (1989). Rheological studies of aqueous amylose gels : The effect of chain length and concentration on gel modulus. *Macromolecules*, *351*(29), 346–351. https://doi.org/10.1021/ma00191a063

Cotter, P., Lopez-Exposito, I., Kleiveland, C., Lea, T., Mackie, A., Requena, T., … Witchers, H. (2015). The impact of food bioactives on health. In P. Cotter, C. Kleiveland, A. Mackie, & D. Swiatecka (Eds.), *The Impact of Food Bioactives on Health*. https://doi.org/10.1007//978-3-319-16104-4

Cryan, J. F., & O'Mahony, S. M. (2011). The microbiome-gut-brain axis: From bowel to behavior. *Neurogastroenterology and Motility*, *23*(3), 187–192. https://doi.org/10.1111/j.1365-2982.2010.01664.x

Den Besten, G., Van Eunen, K., Groen, A. K., Venema, K., Reijngoud, D. J., & Bakker, B. M. (2013). The role of short-chain fatty acids in the interplay between diet, gut microbiota, and host energy metabolism. *Journal of Lipid Research*, *54*(9), 2325–2340. https://doi.org/10.1194/jlr.R036012

Dhital, S., Warren, F. J., Butterworth, P. J., Ellis, P. R., Gidley, M. J., Dhital, S., … Ellis, P. R. (2017). Mechanisms of starch digestion by α - amylase — Structural basis for kinetic properties. *Critical Reviews in Food Science and Nutrition*, *57*(5), 875–892. https://doi.org/10.1080/10408398.2014.922043

Durica-Mitic, S., Göpel, Y., & Görke, B. (2018). Carbohydrate utilization in bacteria: making the most out of sugars with the help of small regulatory RNAs. *Regulating with RNA in Bacteria and Archaea*, (1), 229–248. https://doi.org/10.1128/9781683670247.ch14

Edwards, C. H., Grundy, M. M. L., Grassby, T., Vasilopoulou, D., Frost, G. S., Butterworth, P. J., … Ellis, P. R. (2015). Manipulation of starch bioaccessibility in wheat endosperm to regulate starch digestion, postprandial glycemia, insulinemia, and gut hormone responses: A randomized controlled trial in healthy ileostomy participants. *American Journal of Clinical Nutrition*, *102*(4), 791–800. https://doi.org/10.3945/ajcn.114.106203

Egger, L., Ménard, O., Delgado-Andrade, C., Alvito, P., Assunção, R., Balance, S., … Portmann, R. (2016). The harmonized INFOGEST *in vitro* digestion method: From knowledge to action. *Food Research International*, *88*, 217–225. https://doi.org/10.1016/j.foodres.2015.12.006

Egger, L., Schlegel, P., Baumann, C., Stoffers, H., Guggisberg, D., Brügger, C., … Portmann, R. (2017). Physiological comparability of the harmonized INFOGEST *in vitro* digestion method to *in vivo* pig digestion. *Food Research International*, *102*(July), 567–574. https://doi.org/10.1016/j.foodres.2017.08.047

Englyst, H. N., Kingman, S. M., & Cummings, J. H. (1992). Classification and measurement of nutritionally important starch fractions. *European Journal of Clinical Nutrition*, *46*(2), 30–50

Flint, H. J., Scott, K. P., Duncan, S. H., Louis, P., & Forano, E. (2012). Microbial degradation of complex carbohydrates in the gut. *Gut Microbes*, *August*, 289–306. https://doi.org/10.4161/gmic.19897

Fredriksson, H., Silverio, J., Andersson, R., Eliasson, A.-C., & Åman, P. (1998). The influence of amylose and amylopectin characteristics on gelatinization and retrogradation properties of different starches. *Carbohydrate Polymers*, *35*(3–4), 119–134. https://doi.org/10.1016/S0144-8617(97)00247-6

Gabrielli, V., Kuraite, A., Alves, M., Edler, K. J., Nepravishta, R., García, J. C. M., & Khimyak, Y. Z. (2021). Spin diffusion transfer difference (SDTD) NMR: an advanced method for the characterisation of water structuration within particle networks. *Journal of Colloid And Interface Science*. https://doi.org/10.1016/j.jcis.2021.02.094

Gong, B., Cheng, L., Gilbert, R. G., & Li, C. (2019a). Distribution of short to medium amylose chains are major controllers of *in vitro* digestion of retrograded rice starch. *Food Hydrocolloids*, *96*(March), 634–643. https://doi.org/10.1016/j.foodhyd.2019.06.003

Gong, B., Cheng, L., Gilbert, R. G., & Li, C. (2019b). Distribution of short to medium amylose chains are major controllers of *in vitro* digestion of retrograded rice starch. *Food Hydrocolloids*, *96*(March), 634–643. https://doi.org/10.1016/j.foodhyd.2019.06.003

Gorham, J. B., Williams, B. A., Gidley, M. J., & Mikkelsen, D. (2016). Visualization of microbe-dietary remnant interactions in digesta from pigs, by fluorescence in situ hybridization and staining methods; effects of a dietary arabinoxylan-rich wheat fraction. *Food Hydrocolloids*, *52*, 952–962. https://doi.org/10.1016/j.foodhyd.2015.09.011

Hanashiro, I., Abe, J. I., & Hizukuri, S. (1996). A periodic distribution of the chain length of amylopectin as revealed by high-performance anion-exchange chromatography. *Carbohydrate Research*, *283*, 151–159. https://doi.org/10.1016/0008-6215(95)00408-4

Jacobs, D.M., Deltimple, N., van Velzen, E., van Dorsten, F.A., Bingham, M., Vaughan, E.E., van Duynhoven, J. (2008). 1H NMR metabolite profiling of feces as a tool to assess the impact of nutrition on the human microbiome. *NMR in Biomedicine*, *21*(3), 615–626. https://doi.org/10.1002/nbm

Kaoutari, A. El, Armougom, F., Gordon, J. I., Raoult, D., & Henrissat, B. (2013). The abundance and variety of carbohydrate-active enzymes in the human gut microbiota. *Nature Reviews Microbiology*, *11*(7), 497–504. https://doi.org/10.1038/nrmicro3050

Koev, T. T., Muñoz-García, J. C., Iuga, D., Khimyak, Y. Z., & Warren, F. J. (2020). Structural heterogeneities in starch hydrogels. *Carbohydrate Polymers*, *249*(July), 116834. https://doi.org/10.1016/j.carbpol.2020.116834

Lawson, M. A. E., Neill, I. J. O., Kujawska, M., Wijeyesekera, A., Flegg, Z., Chalken, L., & Hall, L. J. (2019). Infant diet promotes Bifidobacterium community cooperation within a single ecosystem . *BioRXiv*, *July*, 1–42. https://doi.org/https://doi.org/10.1101/711234

Le Gall, G., Noor, S. O., Ridgway, K., Scovell, L., Jamieson, C., Johnson, I. T., … Narbad, A. (2011). Metabolomics of fecal extracts detects altered metabolic activity of gut microbiota in ulcerative colitis and irritable bowel syndrome. *Journal of Proteome Research*, *10*(9), 4208–4218. https://doi.org/10.1021/pr2003598

Le Leu, R. K., Brown, I. L., Hu, Y., Morita, T., Esterman, A., & Young, G. P. (2007). Effect of dietary resistant starch and protein on colonic fermentation and intestinal tumourigenesis in rats. *Carcinogenesis*, *28*(2), 240–245. https://doi.org/10.1093/carcin/bgl243

Li, H., Prakash, S., Nicholson, T. M., Fitzgerald, M. A., & Gilbert, R. G. (2016). The importance of amylose and amylopectin fine structure for textural properties of cooked rice grains. *Food Chemistry*, *196*, 702–711. https://doi.org/10.1016/j.foodchem.2015.09.112

Lockyer, S., & Nugent, A. P. (2017). Health effects of resistant starch. *Nutrition Bulletin*, *42*(1), 10–41. https://doi.org/10.1111/nbu.12244

Minekus, M., Alminger, M., Alvito, P., Ballance, S., Bohn, T., Bourlieu, C., … Brodkorb, A. (2014). A standardised static *in vitro* digestion method suitable for food-an international consensus. *Food and Function*, *5*(6), 1113–1124. https://doi.org/10.1039/c3fo60702j

Moretti, R., & Thorson, J. S. (2008). A comparison of sugar indicators enables a universal high-throughput sugar-1-phosphate nucleotidyltransferase assay. *Analytical Biochemistry*, *377*(2), 251–258.

https://doi.org/10.1016/j.ab.2008.03.018

Muhammad, A., Lamendola, O., Daas, A., Kumar, A., & Vidyarthi, G. (2014). Association between colonic diverticulosis and prevalence of colorectal polyps. *International Journal of Colorectal Disease*, *29*(8), 947–951. https://doi.org/10.1007/s00384-014-1908-9

Namazi, H., Fathi, F., & Dadkhah, A. (2011). Hydrophobically modified starch using long-chain fatty acids for preparation of nanosized starch particles. *Scientia Iranica*, *18*(3 C), 439–445. https://doi.org/10.1016/j.scient.2011.05.006

Peppas, N. A., Bures, P., Leobandung, W., & Ichikawa, H. (2000). Hydrogel in pharmaceutical formulations. *European Journal of Pharmaceutics and Biopharmaceutics*, *50*, 27–46. https://doi.org/10.16953/deusbed.74839

Petropoulou, K., Salt, L. J., Edwards, C. H., Warren, F. J., Garcia-Perez, I., Chambers, E. S., … Frost, G. S. (2020). A natural mutation in *Pisum sativum L.* (pea) alters starch assembly and improves glucose homeostasis in humans. *Nature Food*, *1*(11), 693–704. https://doi.org/10.1038/s43016-020-00159-8

Phan, V. H. G., Trang Duong, H. T., Tran, P. T., Thambi, T., Ho, D. K., & Murgia, X. (2021). Self-assembled amphiphilic starch based drug delivery platform: synthesis, preparation, and interactions with biological barriers. *Biomacromolecules*, *22*(2), 572–585. https://doi.org/10.1021/acs.biomac.0c01430

Purchiaroni, F., Tortora, A., Gabrielli, M., Bertucci, F., Gigante, G., Ianiro, G., … Gasbarrini, A. (2013). The role of intestinal microbiota and the immune system. *European Review for Medical and Pharmacological Sciences*, *17*(3), 323–333.

Raigond, P., Ezekiel, R., & Raigond, B. (2015). Resistant starch in food: A review. *Journal of the Science of Food and Agriculture*, *95*(10), 1968–1978. https://doi.org/10.1002/jsfa.6966

Reeves, A. R., D'Elia, J. N., Frias, J., & Salyers, A. A. (1996). A Bacteroides thetaiotaomicron outer membrane protein that is essential for utilization of maltooligosaccharides and starch. *Journal of Bacteriology*, *178*(3), 823–830. https://doi.org/10.1128/jb.178.3.823-830.1996

Rujivipat, S., & Bodmeier, R. (2010a). Modified release from hydroxypropyl methylcellulose compression-coated tablets. *International Journal of Pharmaceutics*, *402*(1–2), 72–77. https://doi.org/10.1016/j.ijpharm.2010.09.021

Rujivipat, S., & Bodmeier, R. (2010b). Modified release from hydroxypropyl methylcellulose compression-coated tablets. *International Journal of Pharmaceutics*, *402*(1–2), 72–77. https://doi.org/10.1016/j.ijpharm.2010.09.021

Sanchón, J., Fernández-Tomé, S., Miralles, B., Hernández-Ledesma, B., Tomé, D., Gaudichon, C., & Recio, I. (2018). Protein degradation and peptide release from milk proteins in human jejunum. Comparison with *in vitro* gastrointestinal simulation. *Food Chemistry*, *239*, 486–494. https://doi.org/10.1016/j.foodchem.2017.06.134

Silvester, K. R., Englyst, H. N., & Cummings, J. H. (1995). Ileal recovery of starch from whole diets containing resistant starch measured *in vitro* and fermentation of ileal effluent. *American Journal of Clinical Nutrition*, *62*(2), 403–411. https://doi.org/10.1093/ajcn/62.2.403

Sintov, A., Di-Capua, N., & Rubinstein, A. (1995). Cross-linked chondroitin sulphate: characterization for drug delivery purposes. *Biomaterials*, *16*(6), 473–478. https://doi.org/10.1016/0142-9612(95)98820-5

Tao, K., Li, C., Yu, W., Gilbert, R. G., & Li, E. (2019). How amylose molecular fine structure of rice starch affects functional properties. *Carbohydrate Polymers*, *204*, 24–31. https://doi.org/10.1016/j.carbpol.2018.09.078

Tizzotti, M. J., Sweedman, M. C., Tang, D., Schaefer, C., & Gilbert, R. G. (2011). New 1H NMR procedure for the characterization of native and modified food-grade starches. *Journal of Agricultural and Food Chemistry*, *59*(13), 6913–6919. https://doi.org/10.1021/jf201209z

Topping, D. L., & Clifton, P. M. (2001). Short-chain fatty acids and human colonic function: Roles of resistant starch and nonstarch polysaccharides. *Physiological Reviews*, *81*(3), 1031–1064. https://doi.org/10.1152/physrev.2001.81.3.1031

Tu, H., Qu, Y., Hu, X., Yin, Y., Zheng, H., Xu, P., & Xiong, F. (2010). Study of the sigmoidal swelling kinetics of carboxymethylchitosan-g-polyacrylic acid hydrogels intended for colon-specific drug delivery. *Carbohydrate Polymers*, *82*, 440–445. https://doi.org/10.1016/j.carbpol.2010.04.086

Varum, F., Freire, A. C., Bravo, R., & Basit, A. W. (2020). OPTICORE ™ , an innovative and accurate colonic targeting technology. *International Journal of Pharmaceutics*, *583*(February), 119372. https://doi.org/10.1016/j.ijpharm.2020.119372

Vashist, A., Vashist, A., Gupta, Y. K., & Ahmad, S. (2014). Recent advances in hydrogel based drug delivery systems for the human body. *J. Mater. Chem. B*, *2*(2), 147–166. https://doi.org/10.1039/C3TB21016B

Vignoli, A., Ghini, V., Meoni, G., Licari, C., Takis, P. G., Tenori, L., … Luchinat, C. (2019). High-throughput metabolomics by 1D NMR. *Angewandte Chemie - International Edition*, *58*(4), 968–994. https://doi.org/10.1002/anie.201804736

Vilaplana, F., & Gilbert, R. G. (2010). Characterization of branched polysaccharides using multiple-detection size separation techniques. *Journal of Separation Science*, *33*(22), 3537–3554. https://doi.org/10.1002/jssc.201000525

Wang, J. F., Zhu, Y. H., Li, D. F., Wang, Z., & Jensen, B. B. (2004). *In vitro* fermentation of various fiber and starch sources by pig fecal inocula. *Journal of Animal Science*, *82*(9), 2615–2622. https://doi.org/10.2527/2004.8292615x

Warren, F. J., Fukuma, N. M., Mikkelsen, D., Flanagan, B. M., & Williams, B. A. (2018). Food starch structure

impacts gut microbiome composition. *American Society for Microbiology, MSphere*, *3*(3), 1–13.

Williams, Bosch, M. W., Boer, H., Verstegen, M. W. A., & Tamminga, S. (2005). An *in vitro* batch culture method to assess potential fermentability of feed ingredients for monogastric diets. *Animal Feed Science and Technology*, *123-124 Pa*, 445–462. https://doi.org/10.1016/j.anifeedsci.2005.04.031

Williams, C. F., Walton, G. E., Jiang, L., Plummer, S., Garaiova, I., & Gibson, G. R. (2015). Comparative analysis of intestinal tract models. *Annual Reviews of Food Science and Technology*, *6*(14). https://doi.org/10.1146/annurev-food-022814-015429

Witt, T., Gidley, M. J., & Gilbert, R. G. (2010). Starch digestion mechanistic information from the time evolution of molecular Size distributions. *Journal of Agricultural and Food Chemistry*, *58*(14), 8444–8452. https://doi.org/10.1021/jf101063m

Wu, A. C., Li, E., & Gilbert, R. G. (2014). Exploring extraction/dissolution procedures for analysis of starch chain-length distributions. *Carbohydrate Polymers*, *114*, 36–42. https://doi.org/10.1016/j.carbpol.2014.08.001

Ze, X., David, Y. Ben, Laverde-Gomez, J. A., Dassa, B., Sheridan, P. O., Duncan, S. H., … Flint, H. J. (2015). Unique organization of extracellular amylases into amylosomes in the resistant starch-utilizing human colonic firmicutes bacterium ruminococcus bromii. *MBio*, *6*(5), 1–11. https://doi.org/10.1128/mbio.01058-15

CRediT Authorship Contribution Statement

TTK – Conceptualisation, Data curation, Formal analysis, Investigation, Methodology, Writing – original draft, review & editing.

HCH – Methodology, Writing – review & editing.

SK – Data curation.

YZK – Conceptualisation, Methodology, Supervision, Writing – review and editing.

FJW – Conceptualisation, Formal analysis, Funding acquisition, Methodology, Supervision, Writing – review & editing.

Declaration of Conflicts of Interest

There are no conflicts to declare.

Graphical abstract